Engineering Geology 116 (2010) 117–128

Contents lists available at ScienceDirect

Engineering Geology

journal homepage: www.elsevier.com/locate/enggeo

Effect of ductile deformation of quartz-bearing rocks on the alkali-silica reaction

Francisco Locati [a,*], Silvina Marfil [b], Edgardo Baldo [a]

[a] CICTERRA-CONICET-UNC, Av. Vélez Sarsfield 1611 (X5016GCA), Córdoba, Argentina
[b] Departamento de Geología, Universidad Nacional del Sur, San Juan 670 (8000), Bahía Blanca, Buenos Aires, Argentina

ARTICLE INFO

Article history:
Received 9 December 2009
Received in revised form 16 June 2010
Accepted 4 August 2010
Available online 13 August 2010

Keywords:
Microstructure
Petrography
Alkali-aggregate reaction
Expansion
Concrete

ABSTRACT

It has been known for a long time that strained, microcrystalline or cryptocrystalline quartz-bearing aggregates may cause alkali-silica reactions in concrete. Studying the relationship between deformation processes and microstructural characteristics of rocks, the reason for this behaviour can be better understood. Orthogneisses from the metamorphic basement of the Sierra Chica, Córdoba (Argentina), which were locally and differentially deformed in ductile shear zones, were used to analyse such behaviour. Petrographic analyses, accelerated mortar bar tests (ASTM C 1260, 2005) and chemical test (ASTM C 289, 1994) were conducted. Furthermore, corrosion tests were performed on polished rock surfaces using 1 N NaOH solution. It was seen that the reactivity of the quartz-bearing mylonites increased by ~30% with respect to the non-mylonitised sample due to the increment in the strained quartz content and specially with the extended subgrain development. The mylonitised rock affected by superimposed cataclasis and the development of pseudotachylytic veins incremented its reactivity by ~97% with respect to the non-mylonitised sample due to the combined effects of subgrain formation, grain size reduction and the formation of glassy material. It was also the only sample that showed significant differences in surface corrosion confirming the high reactivity of the rock. These results agree with expansion values measured on the accelerated mortar bar test and with silica leached in the chemical test. We believe that the simultaneous use of different tools to evaluate the potential alkali reactivity of the rocks in concrete is a good strategy rather than the use of isolated tools, which could lead to confusing interpretations of the process and therefore result in erroneous decisions.

1. Introduction

Igneous and metamorphic quartz-bearing rocks affected by deformation processes from Buenos Aires and Córdoba provinces are used as concrete aggregates in many parts of Argentina specially in Buenos Aires and Córdoba provinces (Batic et al., 2008), and many studies have been performed in those rocks for many years (e.g. Batic et al., 1987; Cortelezzi et al., 1990; Marfil and Maiza, 2001; Ponce and Batic, 2006; Falcone et al., 2008; Giaccio et al., 2008, among others).

In the Sierras Chicas of Córdoba (Province of Córdoba), the quarries that produce brittle aggregates are located in the eastern side of the range where well and poorly foliated rocks are observed. They are locally affected by centimetric to decametric ductile to brittle-ductile shear zones producing protomylonites to mylonites and centimetric pseudotachylytic veins. Those shear zones are variable in size, with diffuse limits and are interspersed with the surrounding rocks (gneisses, migmatites, granites, etc.) which are the principal target of the quarry. Therefore, different materials affected by variable deformation processes are mixed in the exploitation and milling processes. This problem is similar to that in Scandinavia where cataclastic and strained quartz-bearing rocks are used like aggregate in concrete due to its geological setting (Wigum, 1995).

Since the first work by Stanton (1940a,b), numerous investigations have been conducted in order to design a simple, quick and reproducible method to establish the susceptibility of some rocks to develop alkali-aggregate reactions (AAR).

AAR is a general term to define the expansive reactions between the alkalis in the pore solution in concrete and reactive minerals in the aggregates. This reaction has two forms: (1) alkali-silica reaction (ASR), when the reacting species are varieties of silica minerals, such as strained quartz, opal, trydimite, cristobalite, chert and volcanic glass, which produce expansive alkali-silica gels and (2) alkali-carbonate reaction (ACR) when the aggregates contain alkali and argillaceous dolomitic limestone. In this reaction, the expansion is initiated by a de-dolomitisation processes in the rocks (St. John et al., 1998).

The main source of alkalis is derived from the cement itself, but any source of sodium or potassium can contribute to the reaction. This chemical process can only proceed if all of the three following factors are present in the concrete: (a) sufficient moisture (more than 85% relative humidity) in the pore structure of the concrete, (b) a

* Corresponding author. UNC-FCEFyN, Cátedra de Geología General, Av. Vélez Sarsfield 1611 (X5016GCA), Córdoba, Argentina. Tel.: +54 351 4344980/4981x113; fax: +54 351 4334139.
E-mail addresses: flocati@efn.uncor.edu (F. Locati), smarfil@uns.edu.ar (S. Marfil), ebaldo@com.uncor.edu (E. Baldo).

0013-7952/$ – see front matter © 2010 Elsevier B.V. All rights reserved.
doi:10.1016/j.enggeo.2010.08.001

sufficiently high alkalinity in the pore fluid surrounding the reacting particle and (c) a reactive mineral in the aggregate that often may not react unless it is present in a critical percentage. If any one of these three factors is absent, then the ASR will not proceed (St. John et al., op. cit.).

Alkali ions (and hydroxyl ions from concrete pore solution) can react with the silica in the aggregates to produce alkali silicates that hydrate and increase in volume when water is present. Eventually, these compounds can incorporate calcium forming a more rigid and thicker grain boundary in the aggregate, which acts as a semi-permeable membrane that allows the ingress of alkaline solutions and prevents the release of silicates that continue to be formed inside the aggregate. The process creates internal pressures that are so high that exceed the resistance to internal stress in concrete with the subsequent development of cracks that weaken the structure (Ichikawa and Miura, 2007).

It is possible that the first work studying the reactivity of aggregates with strained quartz was carried out by Mielenz (1954, 1958) and Brown (1955). They revealed that the quartz-bearing rocks with defects in their crystalline structure could behave as potentially reactive aggregates.

Later studies proposed another point of view to approach this problem, focussing mainly on the textural and microstructural characteristics of the rock rather than on their mineralogical composition and petrographic nomenclature (e.g. Gogte, 1973; French, 1991; Grattan-Bellew, 1992; Wigum and Lindgård, 1994; Wigum, 1995). From then on, many research studies have been carried out to find a way of relating these microstructural characteristics to the expansions observed in concrete, particularly in slow-reacting rocks. However, it should be borne in mind that it is necessary to know the geological history, the quartz properties and its potential role to develop the ASR to fully understand the process (Broekmans, 2004b,c).

Dehills and Corvalan (1964) proposed a method to measure the undulatory extinction (UE) angle of strained quartz to evaluate the degree of strain undergone by the rock during the deformation processes. The UE angle is measured by rotating a quartz grain in a thin section under a petrographic microscope and determining the position at which the first clear evidence of undulatory extinction appears and the extinction bands disappear. Some researchers have used this method to correlate mortar bar expansion with quartz deformation effects (Gogte, 1973). However, maybe the most important work was carried out by Dolar-Mantuani (1981), who introduced some changes to the method and established the relationship between the UE angle and the reactivity of rocks in concrete. Although some scientists are still using this method or have suggested some changes (West, 1991, 1994), many of them have questioned it (Grattan-Bellew, 1986, 1992; Andersen and Thaulow, 1989; French, 1992; Thomson and Grattan-Bellew, 1993).

Another tool that has been used by many researchers to establish the potential reactive behaviour of the rocks containing deformed quartz is the Crystallinity Index (CI) (a procedure introduced by Murata and Norman, 1976). Although there is a general tendency to consider that higher CI values are associated with lower concrete expansion values, there are cases in which the observed behaviour is quite the opposite. This is why no good correlation has been established yet and therefore no conclusion has been drawn (Morino, 1986; Katayama and Futagawa, 1989; Thomson and Grattan-Bellew, 1993; Thomson et al., 1994; Wigum, 1995; Wakizaka, 2000; Broekmans, 2004a,b,c; Hünger, 2007).

With time, computerised data processing began to be more frequently used as a complementary tool (e.g. García del Amo and Calvo Pérez, 2001). However, it is worth emphasising that the information obtained should always be critically evaluated and backed by supporting data.

Although many methods to relate the microstructural characteristics of the rocks and the expansions observed in concrete were developed, there is no agreement about which of them would be a reliable tool. Thus, the simultaneous use of different tools appears to be a more reliable criterion.

A deformational history study of the same type of quartz-bearing rocks (orthogneisses of Sierra Chica, Córdoba, Argentina) as well as the right identification and description of their textures, microstructures and mineralogical compositions (in combination with standardised methods) were performed to assess their potential behaviour with respect to the ASR.

2. Dynamic metamorphism, microstructures and reactivity

Temperature and pressure increase with Earth's crust depth. This is defined as the geothermal gradient and may vary depending on the prevailing geological setting, a normal gradient for an intracratonic area being ~25 °C/km (Best, 2003). The rocks that are transported from their place of origin to other depths and stabilised there for a considerable period undergo changes in their texture and mineral composition as a consequence of the new physical conditions (mainly temperature and pressure) and are converted into metamorphic rocks. Within the assemblage of metamorphic rocks, there is a specific group associated with the so-called dynamic metamorphism that develops in localised areas of the crust (shear zones) and undergoes non-coaxial stresses and varying strain rates. This process of rock deformation that accompanies faulting must change with crust depth as a result of varying temperature, fluid pressure and confining pressure, and will also be affected by the velocity mode of the faulting (Sibson, 1977). These shear zones are characterised by the presence of a sequence of rocks that experience deformations under brittle to ductile regimes and develop in planar and approximately parallel structures that begin to anastomose as depth increases.

Fig. 1 shows the conceptual model of a crustal deformation zone as depth increases, changing from cataclastic deformed rocks under a brittle regime, such as breccias or fault gouges (of low pressures and temperatures), to mylonites and finally mylonitic gneisses (at increasing pressures and temperatures). The transition from cataclasites to mylonites represents the passage from the brittle deformation regime to the plastic flow regime, the latter becoming dominant at >300–350 °C for quartz and >450 °C for feldspar (Sibson, 1977, 1990). The formation of microstructures associated with these deformation zones is mainly the result of the temperature reached by the rock, the stress intensity and the strain rate, as well as the mineral composition of the original rock.

A cataclasite grain size may decrease as the deformation stresses increase (always under a brittle to brittle-ductile regime) and even become a pseudotachylyte (a rock with a high content of glassy material formed by friction melting at a high strain rate, Shand, 1916). This is achieved without passing through the ductile deformation stage that forms mylonitic rocks. Pseudotachylytes are formed due to changes in strain rate rather than in the geothermal gradient (in this case deformation varies within the same structural level). Likewise, a mylonitic rock could grade to an ultramylonitic one due to changes in the intensity of the prevailing stresses. On the other hand, mylonite could evolve into mylonitic gneiss or blastomylonite if the geothermal conditions are adequate, with the subsequent recrystallisation and dislocation removal. In the latter case the structural level varies towards higher pressure and temperature conditions.

In general, at a higher degree of internal deformation the rock experiences a higher expansion in the concrete, which may be attributed to the development of crystal discontinuities in quartz (Wigum, 1995) and to metamorphic foliation development (Kerrick and Hooton, 1992). However, other variables of the deformation and metamorphic processes are to be taken into account, such as the prevailing pressure and temperature during deformation, which could also change their potentially reactive behaviour.

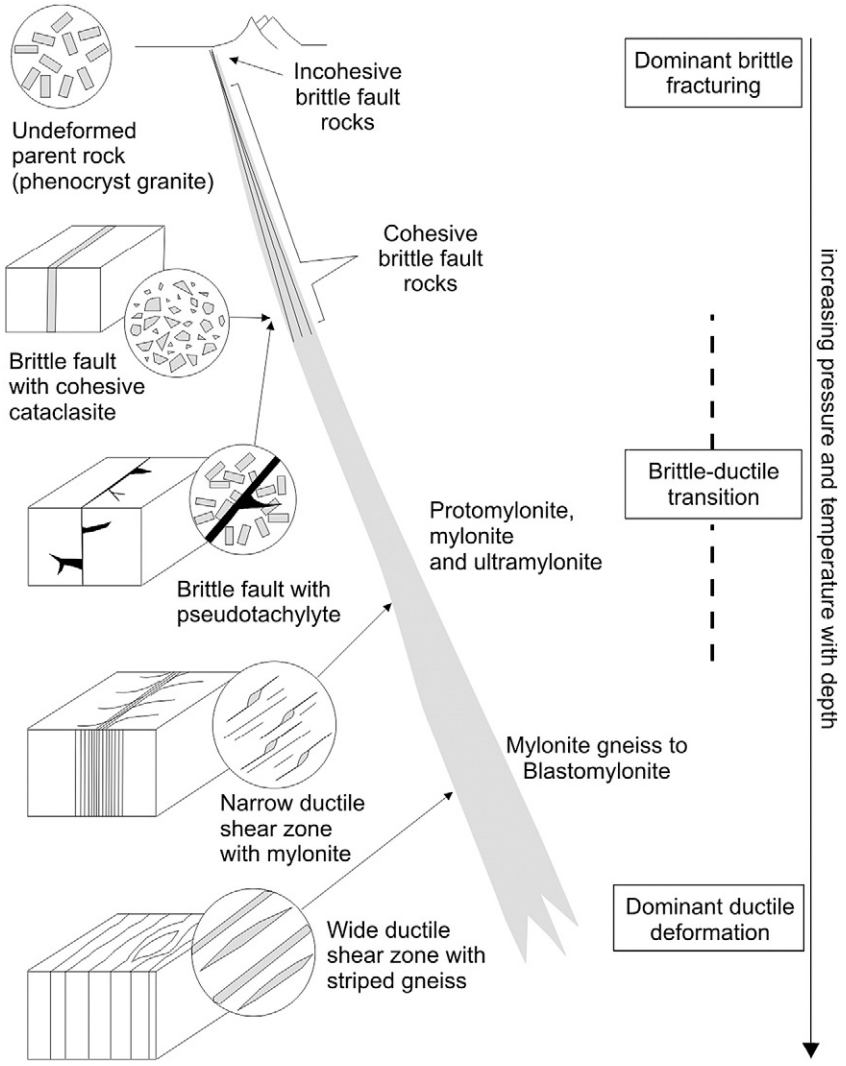

Fig. 1. Distribution of the main fault rocks (out of scale) as a function of the Earth's crust depth (modified from Passchier and Trouw, 2005). The transition between ductile and brittle deformation domains depends on several factors, such as the rock composition, the geothermal gradient and the total strain rate among others.

Through TEM (transmission electron microscopy) images of quartz grains in granitic rocks, Wenk et al. (2008) saw that there was an increase in dislocation density with increasing deformation of the rocks. They also found a positive correlation between the expansion (according to ASTM C 1260, 2005) and dislocation density of these rocks, suggesting that dislocations might play a major role in determining the reactivity of quartz-bearing rocks with respect to the ASR.

At present, there is an extensive and integrated bibliography where the deformation, recovery and crystalline recrystallisation processes are explained in detail. For a more thorough study of these processes and background information on this subject, see Vernon (2004) and Passchier and Trouw (2005).

The defects in the quartz crystalline lattice caused by stresses that lead to intracrystalline deformation (Hull, 1975; Poirier, 1985) are generally related to dislocation development (White, 1973). The clearest example is the undulatory extinction of minerals when the slide is rotated on a petrographic microscope to view them under crossed nichols. The deformation energy associated with dislocations increases the free energy of the crystal and hence dislocations are unstable defects (Hobbs et al., 1976), and it is there where the ASR processes start (Zhang et al., 1990; French, 1991; Kerrick and Hooton, 1992; Ponce and Batic, 2006).

During deformation, ordering and disordering mechanisms compete; when they stop, the ordering mechanisms evolve to reach an equilibrium state. In response to these so-called recovery mechanisms (Hobbs et al., 1976), dislocations tend to concentrate on planar zones in the crystal, reducing the dislocation density in other crystal areas and forming deformation bands (Spry, 1969).

Dislocations in a crystal can be grouped into planar walls of organised dislocations as a result of recovery processes. These networks are known as subgrain walls or subgrain boundaries (Chalmers, 1959; Kingery, 1960; Spry, 1969; Hobbs et al., 1976).

Finally, it is important to understand the recrystallisation process as a way to reduce the dislocation density and hence the degree of internal crystal deformation. As it develops, new smaller size crystals of different shapes and orientations are formed (Poirier and Guillopé, 1979; Urai et al., 1986; Hirt and Tullis, 1992; Passchier and Trouw, 2005; Wang et al., 2007).

Wigum (1995) also mentions inclusions (a fluid or a solid included in the grain of another mineral), myrmekites (symplectic intergrowth of vermicular quartz and plagioclase) and the deformation lamellae (crystallographically oriented narrow and planar zones defined by dislocation walls or varying dislocation bands and fluid inclusion concentration) as the possible sites where the ASR can start.

The decrease of the internal free energy due to dislocation removal in the recrystallisation process could decrease the potential reactivity of the aggregate. However, another variable appears, such as grain-size reduction and the subsequent increase of the specific surface area.

The variables that make the grain size cause a reactive or pozzolanic effect on concrete are well summarized in Wigum et al. (2006) report.

In the recovery and recrystallisation processes during dynamic metamorphism, the inflow of fluids through dislocations or grain boundaries play an important role (Menegon et al., 2008). Likewise in those processes involving dissolution, reaction and nucleation of new phases related to the ASR in concrete, the ingress of alkalis through these channels (French, 1992; Lagerblad and Trägårdh, 1992) as well as through the foliation planes of the rock (Kerrick and Hooton, 1992; Ponce and Batic, 2006) are also necessary.

3. Geological setting and characterisation of materials

The samples of the studied rocks were collected from Las Bateas, a town that is 1.5 km west of La Calera city and belongs to the central region of the igneous-metamorphic basement of the Sierra Chica, Córdoba, Argentina (Fig. 2), of basically Lower Cambrian age (Rapela et al., 1998). The samples come from an orthogneissic lenticular body elongated in the north–south direction, about 5.5 km long and 1 km wide. To the west it limits with tonalitic orthogneisses, and to the east with diatextic migmatites. The development of the ductile shear zone of La Estanzuela, which crosses the boundary of two lithologic domains, can be seen in this area. The La Calera Group, to the east, is composed of migmatites, gneisses, calc-dolomitic marbles and amphibolites; and the El Diquecito Group, to the west, is made up of pyroxenic orthogneisses, tonalitic to granodioritic orthogneisses, and metasedimentary rocks in lower proportion (Baldo et al., 1996; Rapela et al., 1998; Bonalumi et al., 1999). The ductile shear zone of La Estanzuela affects the east boundary of orthogneiss, which is in contact with migmatites, marbles and amphibolites mainly, leading to the mylonitisation of these rocks. Superimposed on the mylonitic foliation, there are cataclasis processes and pseudotachylytic vein developments of varying thickness (≤15 cm) and changing orientation, almost always discordant with the predominant foliation.

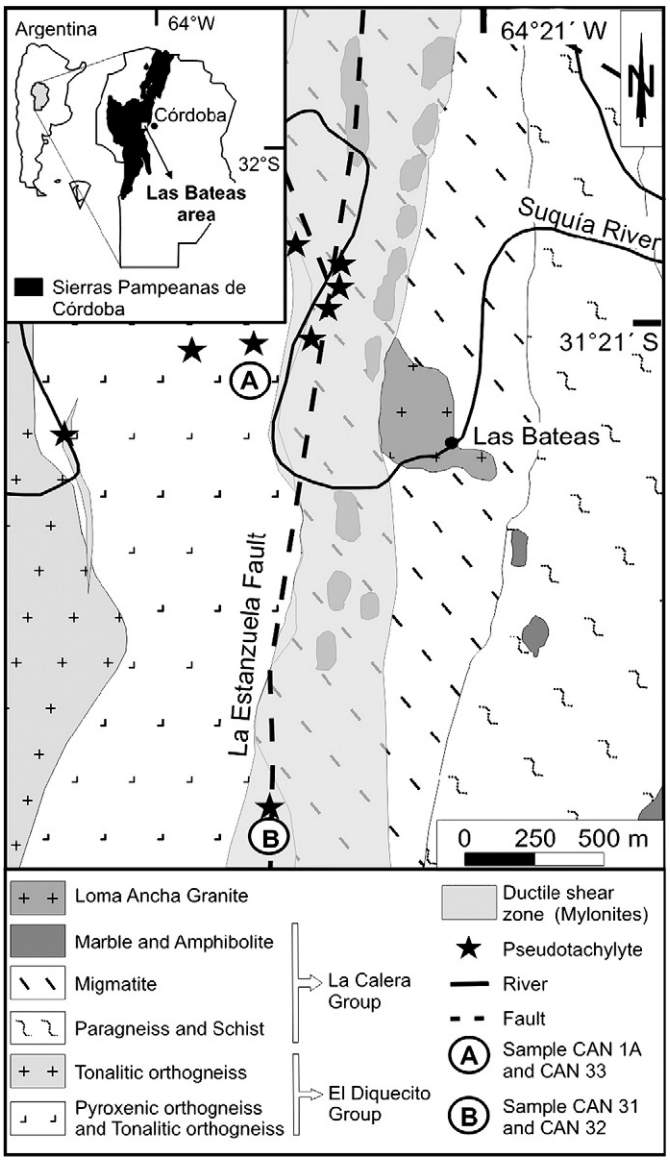

Fig. 2. Lithologic sketch map and location of CAN 1A, CAN 31, CAN 32 and CAN 33 samples from Las Bateas area (lithologic map modified from Gordillo and Lencinas, 1979).

Orthogneiss generally shows a granoblastic texture (Fig. 3a) with xenoblastic, equant and predominantly polygonal grains, which becomes mylonitic owing to ductile deformation processes (Fig. 3b) and sometimes can even be ultramylonitic (Fig. 3c) in maximum deformation zones. In localised areas, where brittle to brittle-ductile deformation prevails, the rock exhibits brecciated texture with reduction in the quartz grain size as a result of basically cataclastic processes, and pseudotachylitic veins develop in the areas where the strain rate is higher (Fig. 3d).

There are different compositional subtypes; the pyroxenic type, which is the most common, contains plagioclase (50–53%), quartz (10–15%), pyroxenes (17–19%), biotite (5–8%), amphibole (5–8%) and opaque minerals (3–5%) as principal minerals, and potassium feldspar, apatite and zircon as accessory minerals (Gordillo, 1958). The other subtypes contain varying proportions of those minerals and can also contain garnet, allanite, epidote, chlorite, sericite, calcite and titanite.

The rock without mylonitic deformation has a medium grain size (approximately 1–3 mm), which notably decreases in the mylonitised zones reaching very fine grain sizes (30 μm or smaller). It is worth mentioning that such grain size does not include subgrains, which are of outmost importance for this study and will be detailed further on. Intergranular contacts are polygonal for both lower deformation and advanced recrystallisation stages, although at intermediate stages the development of sutured or tortuous contacts is common. The rock is basically homogeneous and equigranular, but as deformation processes develop, the grain size distribution approaches a bimodal distribution due to porphyroclastic texture. This texture is the result of the size reduction of some weak minerals as compared to others that are more resistant.

In the samples affected by mylonitisation processes, there is an increase of secondary minerals (epidote, calcite, chlorite, sericite) resulting from the alteration of the original minerals in the rock, which has been possibly favoured by the inflow of hydrothermal fluids.

Pseudotachylytic veins exhibit clear contacts with mylonites, and small plumes or tongues of the melted material invading the host rock are commonly seen. The pseudotachylytic vein can be divided into two areas: the outer area, which is darker and has isotropic optical properties where 15% to 20% of the original rock fragments are still present; and the inner area, which is thicker, dark brown with the formation of acicular and idiomorphic microliths, most of which are organised in a radial arrangement. Relict fragments of the original rock (mainly quartz with undulatory extinction and plagioclase) covered by a thin layer of dark material similar to that of the outer area of the vein are also present.

In previous XRD analyses on pseudotachylytes (Locati et al., 2008), the presence of quartz, potassium feldspar, plagioclase and phyllosilicates of the biotite series could be identified. It should be borne in mind that the analysed fraction belongs both to the melted material and to relict fragments inside the vein. An increase from 20° to 30° 2θ (Cu Kα radiation) in the background values of the plot and peak widening can be observed. This is due to the presence of amorphous or low crystallinity material, which can be attributed to the vitrified

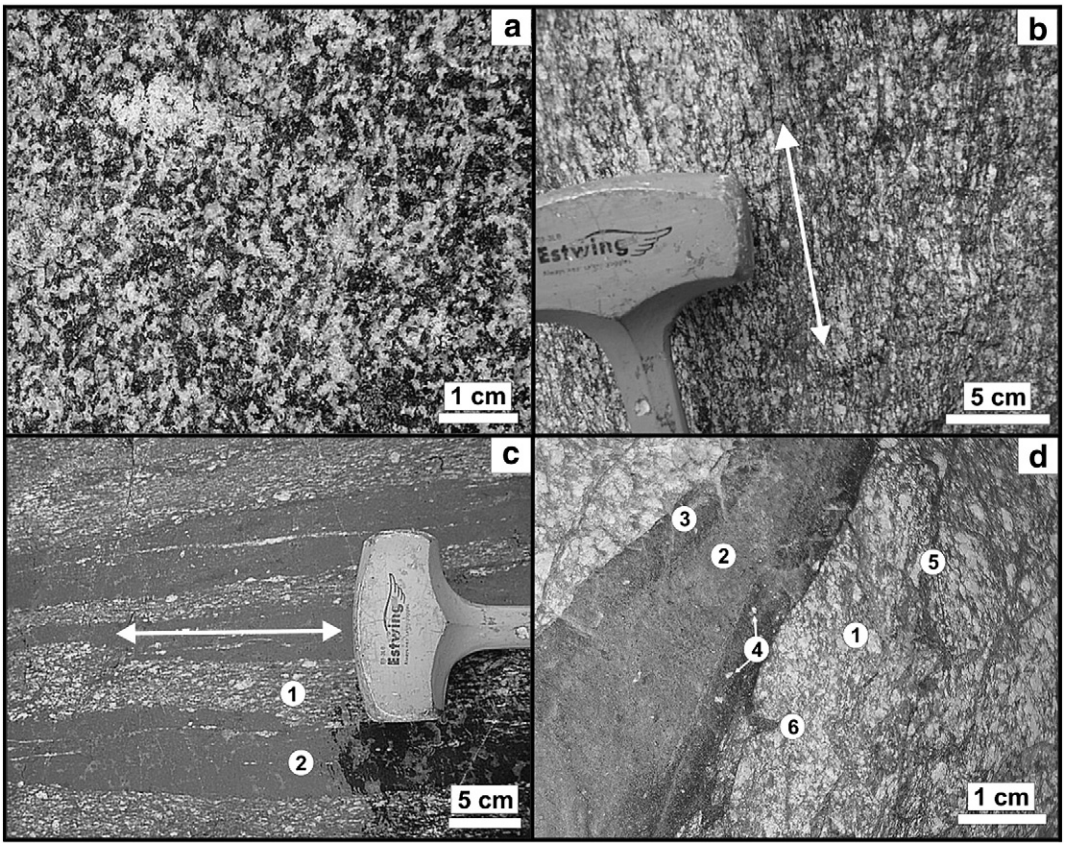

Fig. 3. Macroscopic photographs of the samples. a) CAN 1A sample. Pyroxenic orthogneiss (with no signs of mynolitic deformation and homogeneous and equigranular appearance. b) CAN 31 sample. Protomylonitic pyroxenic orthogneiss. Foliation (arrow) essentially defined by the orientation of mafic minerals is observed. c) CAN 32 sample. Pyroxenic orthogneiss with alternating sectors of strong foliated mylonites (1) and ultramylonites (2). Both sectors are parallel, which indicates that they are coeval. d) CAN 33 sample. Mylonitised and cataclasised pyroxenic orthogneiss (1). Superimposed ductile and brittle deformation events with development of a black pseudotachylytic vein (2–3 cm wide). Straight boundaries can be seen. Inside of the pseudotachylytic vein, a lighter central area that has undergone recrystallisation (2) and a darker boundary, of glassy appearance and without recrystallisation, on both sides of the central area can be distinguished (3). From the original rock, only small white isolated relict fragments are present (4). Abundant smaller veins can also be observed (5) as well as some tongues of the material that invade the mylonite (6).

fraction resulting from the melting of pseudotachylyte that did not undergo subsequent recrystallisation.

In the Las Bateas area (Fig. 2), two deformation processes — the ductile and the brittle — are superimposed. The ductile deformation processes form the microstructures associated with strained quartz, whereas brittle or brittle-ductile processes contribute the micro-discontinuities associated with cataclasis and sometime glass formation resulting from friction melting. Based on previous experiences, such glass could behave in a similar way to the glass in volcanic rocks owing to its chemical instability in alkaline solutions (Locati et al., 2008).

4. Methods

Petrographic analyses of the different types of rocks studied were performed on thin sections under petrographic microscope with polarized light. These analyses were focussed on the textural, mineralogical and microstructural characteristics.

Accelerated mortar bar tests were conducted at 16 days according to ASTM C 1260 (2005) and they were extended to 28 days to identify intermediate behaviours, especially when slow-reacting rocks are analyzed (Falcone et al., 2008). The test consists in moulding cement and sand bars (25×25×285 mm) with grain sizes, proportions, w/c ratio and mixing determined using the aggregates to be evaluated. The bars are first cured in a fog room (24 h), then demoulded and immersed in water at 23 °C in a sealed container and placed in a heater at 80 °C (24 h). Once the (initial) length has been measured, they are immersed in a 1 N NaOH solution at 80 °C for 14 days (a total of 16 test days) and the rest of the readings are taken. The standard prescribes that expansions below 0.10% at 16 days indicate aggregates of innocuous performance, and expansions above 0.20% a potentially deleterious behaviour. For expansions between 0.10% and 0.20% the aggregates are considered as marginal and it is recommended that supplementary information be gathered or further studies be made to be able to discriminate between innocuous and deleterious aggregates. Subsequently, petrographic analyses were performed on thin sections of the bars tested.

Dissolved silica was evaluated by the chemical test method (ASTM C 289, 1994), which consists in crushing a fraction of the aggregate to be evaluated (between 300 μm and 150 μm in size). This fraction is then placed in a sealed container with a 1 N NaOH solution at 80 °C for 24 h; the solution is then filtered and the dissolved silica in the liquid phase is determined.

Corrosion tests were conducted on polished surfaces of the rocks studied in order to determine their susceptibility to alkali attack. Rock pieces were cut (2×4×0.4 cm) and polished with abrasives, mesh No. 1000 (10 μm). Subsequently, they were immersed in a 1 N NaOH solution and placed in a heater at 80 °C for 72 h. Every 24 h they were withdrawn from the heater, washed and viewed with a reflected-light petrographic microscope. Then, they were compared with the non-attacked sample taken as the reference, always working in the same area of the sample (Marfil et al., 1998; Maiza et al., 1999).

Images on a grey scale, with a resolution of 760×570 pixels, were taken from each sample. The luminosity value of each pixel depends on its shade on the grey scale (from black to white). From that matrix, composed of 433,200 points, 6 rows were selected to calculate the luminosity average value (Table 2). With these data, a statistical

analysis was conducted applying the analysis of variance (ANOVA) method of two hierarchically different ways (Steel and Torrie, 1981). In order to compare surface corrosion changes of each sample at different times, Fisher's Least Significant Difference (LSD) was used (Steel and Torrie, op. cit.).

The analysed samples belong mostly to the types with higher deformation from the ductile shear zone of La Estanzuela.

5. Microstructural characterisation of quartz

5.1. Orthogneiss not affected by the mylonitic zone (CAN 1A sample)

The prevailing quartz grain size is from 1 to 3 mm with polygonal contacts. Here, the main microstructure recognised is a slight undulatory extinction. There are also abundant fluid inclusions and less frequent solid inclusions. This pattern also occurs in the rest of the samples analysed.

Recrystallisation processes are incipient and are characterised by the growth of some grain boundaries at the expense of neighbouring grains (irregular boundaries). Subgrains are in a very incipient stage of formation (Fig. 4a and b).

5.2. Orthogneiss weakly affected by the mylonitic zone (CAN 31 sample)

The prevailing quartz grain size is from 1 to 2 mm (although pseudo-grains some tens of micrometres long start to appear). In this deformation stage, there is a pronounced presence of grains with undulatory extinction and deformation bands, formation of pseudo-grains and recrystallised grains associated with recovery and recrystallisation processes (Fig. 4c to e).

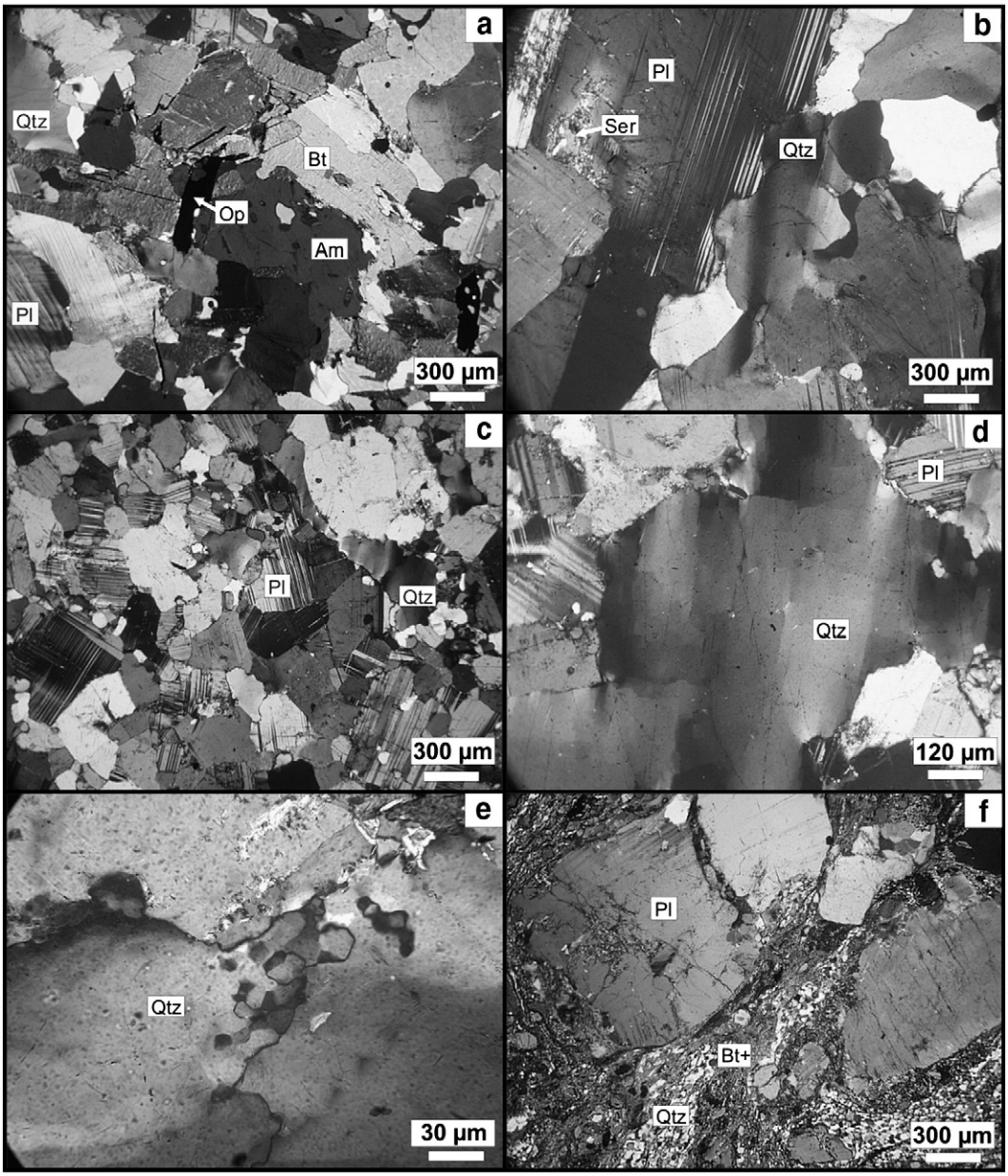

Fig. 4. Photomicrographs of the natural samples under crossed nichols. CAN 1A sample: a) Grano-nematoblastic texture with straight intergranular contacts and a polygonal trend. b) Quartz with undulatory extinction and slightly recrystallised boundaries. CAN 31 sample: c) Grain-size reduction and increase of quartz with undulatory extinction and deformation bands. d) Quartz with blocky extinction and irregular grain boundaries. e) Formation of subgrains and recrystallised grains. CAN 32 sample: f) Mylonite with plagioclase porphyroclasts in a biotite-rich matrix and oriented quartz stripes. Mineral symbols: Qtz: quartz, Bt: biotite, Pl: plagioclase, Ser: sericite, Cal: calcite, Kfs: K-feldspar, Ep: epidote, Am: amphibole, Op: opaque mineral, G: glass, Bt+: biotite + chlorite + calcite + epidote + quartz + plagioclase + K-feldspar.

5.3. Orthogneiss strongly affected by the mylonitic shear zone (CAN 32 sample)

The rock shows marked mylonitic foliation, evidenced by elongated quartz stripes arranged in parallel with the orientation of the matrix biotite sheets and plagioclase porphyroclasts (1–6 mm). This causes the distribution of the grain size to be bimodal. The striped domains are mainly composed of small quartz subgrains (≤30 μm) and polygonal recrystallised quartz of similar size.

It is important to point out that whereas the advanced recrystallisation processes cause a decrease in the high free-energy areas (subgrain boundaries), the grain size continues to be one of the main variables at this stage (grain-size reduction by recrystallisation) (Figs. 4f, 5a and b).

5.4. Orthogneiss affected by superimposed mylonitisation, cataclasis and pseudotachylytic veins formation processes (CAN 33 sample)

The rock shows microstructures associated with ductile deformation processes (quartz with undulatory extinction, subgrain formation and grain recrystallisation) similar to those observed in CAN 31 and CAN 32 samples. Microstructures caused by brittle deformation, such as pulverised quartz formed by cataclasis with very small grain sizes (<10 μm) also occur, as well as the formation of glassy material caused by melting of the original rock (Fig. 5c to f). The glassy material exhibits low thermodynamic stability that under strongly alkaline pH conditions can release different ions into the concrete pore solution.

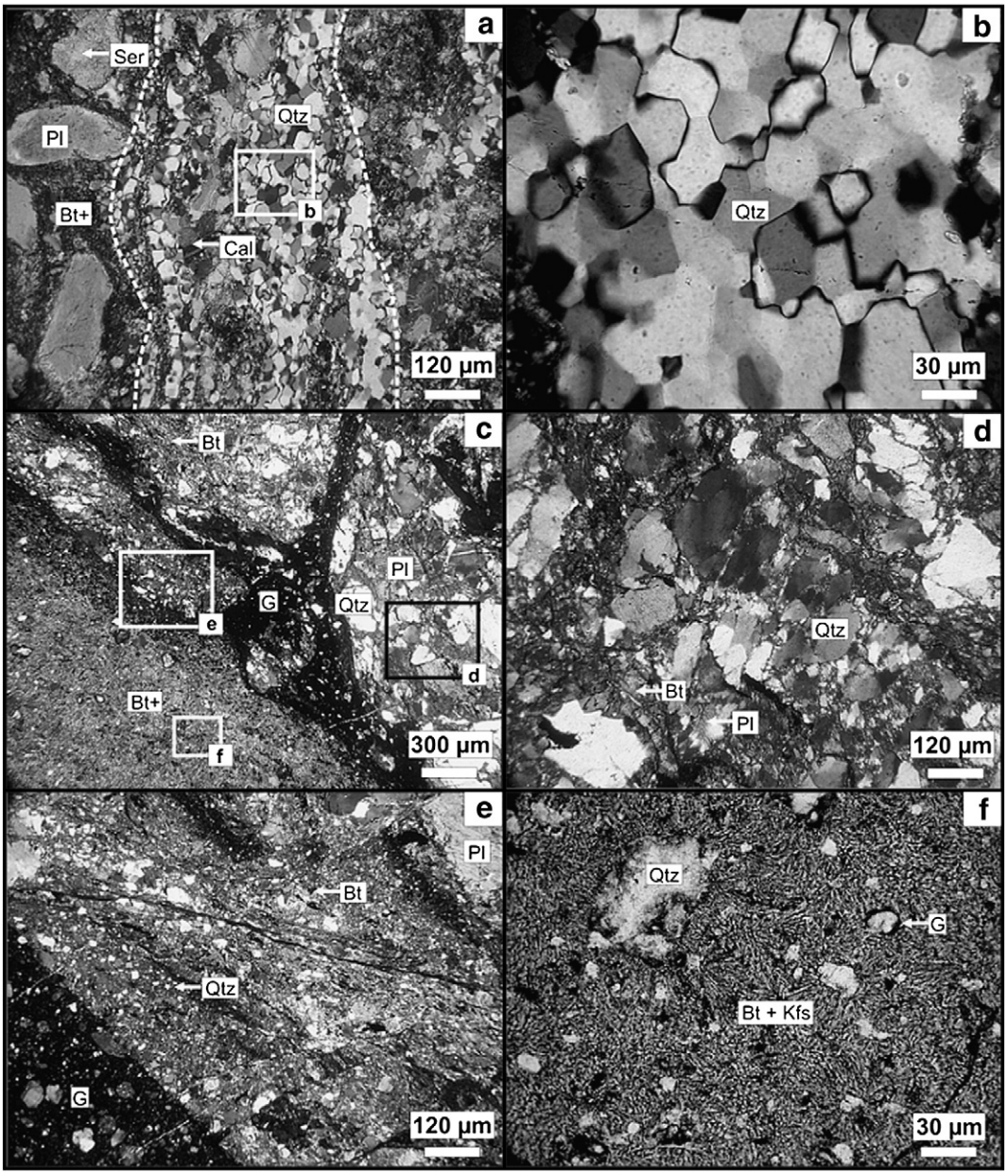

Fig. 5. Photomicrographs of the natural samples (a–e, crossed nichols; f, parallel nichols). CAN 32 sample: (a) Quartz stripe (between white dotted lines) formed by subgrains and grains of polygonal, recrystallised quartz ≤30 μm (b) Details of subgraining and polygonization. CAN 33 sample: c) Pseudotachylyte boundary area. The glassy material (black) invades the mylonite. d) Details of the cataclasised mylonite: Quartz with undulatory extinction and destruction of grain boundaries due to pulverisation during cataclasis. e) Details of the contact between the glassy material and the strongly pulverised mylonite (<10 μm). In the glassy fraction there are small relict mylonitic clasts. f) Details of the recrystallised internal area. Relict clasts with a black boundary of non-recrystallised glass are observed in a matrix composed of biotite microliths and potassium feldspar that occasionally form spherulites. Mineral symbols as in Fig. 4.

6. Results

The threshold limits set by CIRSOC 201 (2005, Draft Regulations of the Research Centre of National Safety Regulations for Civil Works in Argentina) to classify as innocuous aggregates containing volcanic glass in volcanic rocks and aggregates containing strained, microcracked and microcrystalline quartz are ≤3% and ≤5%, respectively.

By petrographic analyses of crushed fractions, it was determined that all the samples exceed 5% of strained quartz, which is the threshold limit (CIRSOC 201). The glass content in the CAN 33 sample is of about 4%, surpassing the limit set for volcanic glass.

The samples tested by the accelerated mortar bar test method (ASTM C 1260, 2005) showed different behaviours, depending on the degree and type of deformation undergone by the rock. All samples showed expansions greater than 0.10% at 16 days (Fig. 6), so the test was extended to 28 days (ASTM C 1260, 2005; Wigum and French, 1996; Falcone et al., 2008). Expansion data on mortar bars and dissolved silica of CAN 33 sample were taken from Locati et al. (2008).

Three different behaviours are generally observed. The non-mylonitised orthogneiss (CAN 1A sample) showed expansions above 0.10% at 16 days, but did not exceed the limit of 0.20% at 28 days. The weakly mylonitised orthogneiss (CAN 31 sample) gave expansions higher than 0.10% and 0.20% at 16 days. The strongly mylonitised orthogneiss (sample CAN 32) showed expansions above 0.10% at 16 days and surpassed the 0.20% threshold value at 28 days. The mylonitised, cataclasised orthogneiss having pseudotachylytic veins (CAN 33 sample) expanded by more than 0.10% and 0.20% at 16 days. The dissolved silica values in the solutions (ASTM C 289, 1994) increase from sample CAN 1A to CAN 33 (Table 1).

Petrographic analyses on thin sections of mortar bars after test time had elapsed show progressive deterioration of the cement paste as more deformed material is added. The aggregate boundaries are generally net but become diffuse when quartz aggregates are analysed, as a result of dissolution (Fig. 7a). There are narrow microcracks in the cement paste with and without filling but they are very scarce and unimportant. However, they are more noticeable in the CAN 33 sample (Fig. 7b). Some cavities are partially filled with a fibrous mineral and sometimes with an amorphous material.

After surface corrosion studies (Figs. 8 and 9) and from luminosity data for each sample (Table 2), a statistical analysis was conducted by the analysis of variance method (Table 3). The results show that there are significant differences in the behaviour of the four samples studied with respect to alkali attack. In addition, although all the samples behave differently, only the CAN 33 sample statistically shows significant evidence of corrosion during test time.

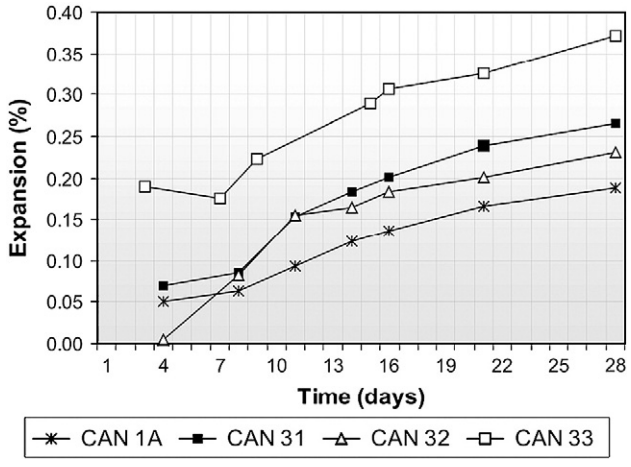

Fig. 6. Progress of mortar bar expansion under the accelerated test method ASTM C 1260 (2005). The lowest expansion values correspond to the mortar made with the non-mylonitised orthogneiss aggregates (CAN 1A sample), and the highest expansion values to the mylonitised, cataclasised orthogneiss with pseudotachylyte veins (CAN 33 sample). All samples show expansions higher than 0.10% at 16 days.

Table 1
Dissolved silica values under the test conditions of ASTM C 289 (1994). Values increase as rock deformation processes intensify.

Sample	Dissolved silica (mg/100 ml)	Dissolved silica (mmol/l)
CAN 1A	3.3	11.00
CAN 31	5.9	19.66
CAN 32	6.2	20.66
CAN 33	11.8	39.42

7. Discussion

Although all the rocks studied surpassed the limit set by the standard for the maximum content of strained quartz-bearing aggregates in the concrete, it is observed once again that the microstructural characteristics rather than the petrographic classification determine their reactive behaviour.

According to Wenk et al. (2008), the ASTM C 1260 (2005) test is a good tool to evaluate the potential alkali reactivity of aggregates and it is an indirect way to measure the degree of internal deformation (and dislocation density) of the rocks. However, the utilization of crossed information (such as dissolved silica values, petrographic analysis, etc.) is also needed to assess the potential alkali reactivity of deformed quartz-bearing rocks.

Non-mylonitised orthogneiss exhibits quartz with undulatory extinction only and hence the degree of internal deformation is possibly not as high as in the mylonites analysed. In the latter there is subgraining or intense recrystallisation processes, which results in higher expansion in the mortar bars due to reduction in the grain size and increase in the total available grain boundary area of quartz (Grattan-Bellew, 1992; Wigum, 1995).

The microstructural difference between weakly mylonitised and strongly mylonitised orthogneiss seems to be related to the development of the recrystallisation processes in quartz. Higher expansion values were expected in the strongly mylonitised rock than in the weakly mylonitised one, and although the values at 28 days were very close (0.231% and 0.265%, respectively), the latter rock expanded more than the former. According to Wigum (1995), the recrystallisation of quartz will decrease the reactivity of the rocks due to amalgamation of smaller grains into larger ones, leading to a smaller total grain boundary area of quartz. The amalgamation of smaller grains into larger ones occurs when the geothermal gradient increases (Vernon, 2004). In our samples there is no increase in the grain size because the process that governs recrystallisation is not an increase in the geothermal gradient but a recovery process of the subgrains into real small grains. Thus, although in the samples studied there is an increase in the specific surface area from the weakly mylonitised to the strongly mylonitised sample (since smaller grains are formed during recrystallisation), the reduction in the dislocation density is possibly the process that mainly determines the decrease in the reactivity of the strongly mylonitised sample.

The mylonitised, cataclasised orthogneiss containing pseudotachylytic veins is the most complex sample since it shows superimposed ductile and brittle deformation processes. Microstructural characteristics such as the presence of pulverised and strained quartz, and glassy material increase their potential reactivity. This is shown by the higher expansion values measured on the mortar bars both at 16 (0.307%) and 28 days (0.372%).

The dissolved silica content increases as the rock deformation processes develop. However, the values do not show the above-mentioned behaviour observed in CAN 31 and CAN 32 samples in the accelerated mortar bar test. It is possible that the aggressive conditions set in the chemical test may give us an idea of the

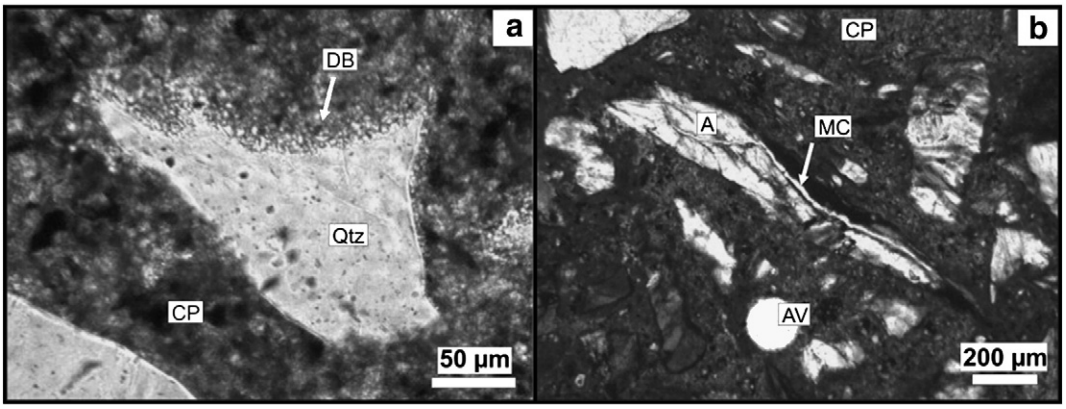

Fig. 7. Photomicrographs of the mortar bars tested. a) CAN 1A sample. Quartz aggregate with dissolved boundaries. b) CAN 33 sample. Microcrack crossing the cement paste and the aggregate. Qtz: quartz, CP: cement paste, DB: dissolved boundary, A: aggregate, MC: microcrack, AV: air void.

maximum silica content that rocks could release into the alkaline solution, but in a long period of time and far away from the 28 days prescribed in the mortar bar test.

All the samples continue expanding without being stabilised on test completion at the age of 28 days, which would be indicative of a slow reaction trend.

Corrosion test results agree with those from the mortar bar and chemical tests. The CAN 33 sample was the one that showed significant leaching on the attacked surface.

Table 4 summarises the relevant information to be taken into account when a deformed quartz-bearing rock is to be characterised with respect to the ASR, based on laboratory experiences. Its classification is qualitative and the use of simultaneous methods such as the accelerated mortar bar test, chemical method, corrosion test and petrographic analysis will contribute to quantifying the behaviour of the rocks. However, more analyses and the study of more samples are needed to confirm these statements.

8. Conclusions

It was observed that the reactivity of quartz-bearing rocks depends mainly on their textural and microstructural characteristics and therefore on the geological processes generating them. The results of this work are summarized as follows.

The reactivity of the quartz-bearing mylonites increased by ~30% with respect to the non-mylonitised sample due to the increment in the strained quartz content and specially with the extended subgrain development.

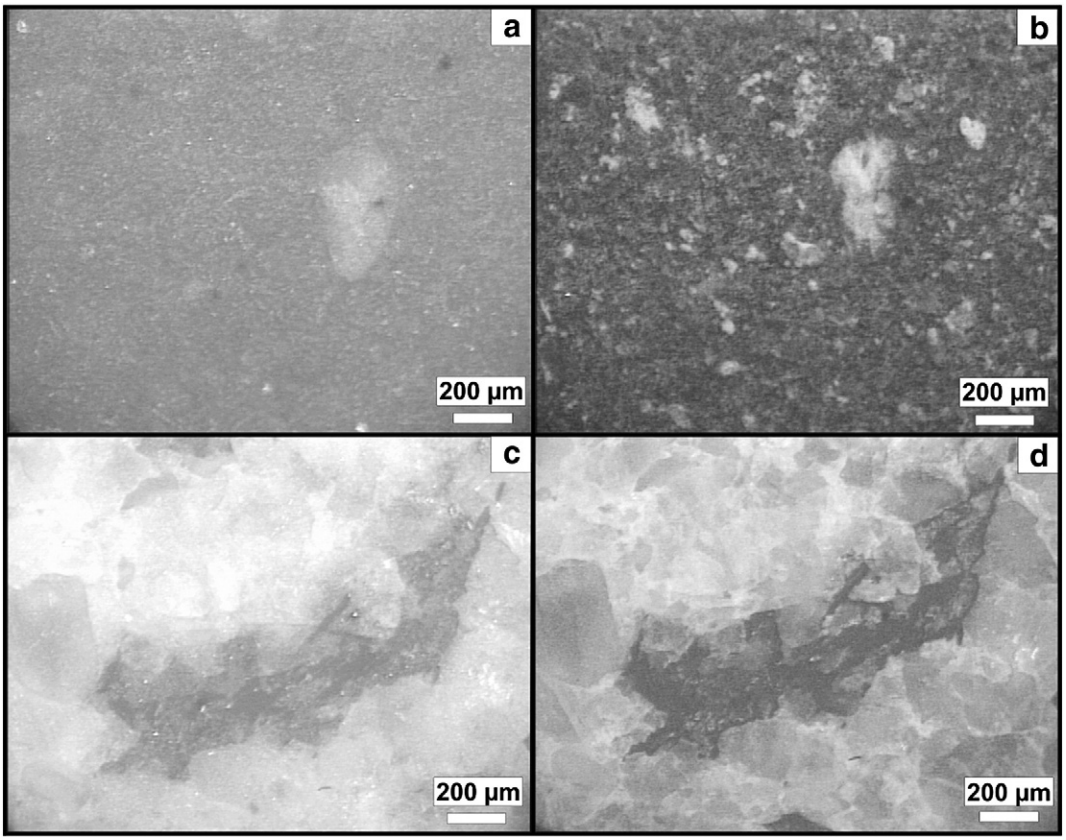

Fig. 8. Photographs viewed with a petrographic microscope under reflected light. CAN 33 sample, precorrosion (a) and postcorrosion (b). CAN 31 sample, precorrosion (c) and postcorrosion (d).

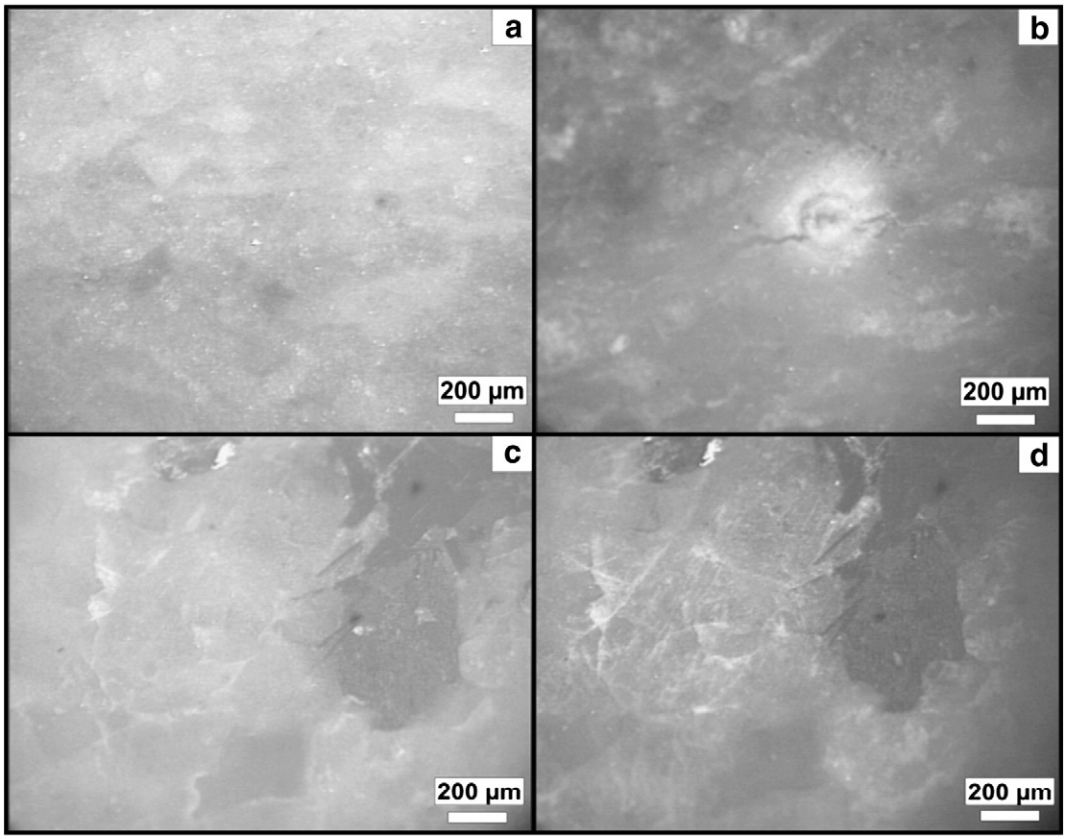

Fig. 9. Photographs viewed with a petrographic microscope under reflected light. CAN 32 sample, precorrosion (a) and postcorrosion (b). CAN 1A sample, precorrosion (c) and postcorrosion (d).

The mylonitised rock affected by superimposed cataclasis and the development of pseudotachylytic veins incremented its reactivity by ~97% with respect to the non-mylonitised sample due to the combined effects of subgrain formation, grain size reduction and the formation of glassy material.

Corrosion tests indicate that the four rocks behave differently with respect to the alkali attack. However, the only sample that showed significant differences in surface corrosion is the mylonite with pseudotachylytic veins confirming its high reactivity.

These results agree with expansions measured on the accelerated mortar bar test and with silica leached in the chemical test.

Table 2
Average luminosity values for each sample as a function of the rate of alkali attack and 5% LSD results into each rock.

Sample	Time (h)	Media	LSD
CAN33	0	78,4132	a
CAN33	24	80,5870	ab
CAN33	48	83,4040	bc
CAN33	72	87,0509	c
CAN31	0	102,7985	b
CAN31	24	93,7236	a
CAN31	48	93,9920	a
CAN31	72	96,4760	a
CAN32	0	100,2969	a
CAN32	24	100,0449	a
CAN32	48	102,3030	a
CAN32	72	99,1003	a
CAN1A	0	91,3716	a
CAN1A	24	95,1601	a
CAN1A	48	94,2419	a
CAN1A	72	93,4065	a

We believe that the simultaneous use of different tools to evaluate the potential alkali reactivity of the rocks in concrete such as petrographic analyses, dissolved silica values, expansion values from the accelerated mortar bar test and corrosion of the polished rock surfaces, is a good strategy rather than isolated tools, which could lead to confusing interpretations of the process and therefore result in erroneous decisions.

Acknowledgements

The authors gratefully acknowledge Universidad Nacional del Sur, Universidad Nacional de Córdoba, CIC from Buenos Aires and CONICET for their support. They also thank Salomón R.C.J. and Dr. Pedro Maiza from the Universidad Nacional del Sur and Mathematics Department from the Universidad Nacional del Sur, for their collaboration. Finally we are grateful to Giovanni B. Crosta (Editor-in-Chief) and anonymous reviewers for their comments that have improved the manuscript.

Table 3
Results of the statistical analyses performed by the analysis of double variance method (ANOVA, two way split-plot design).

Source of variation	Sum of squares (SS)	Degrees of freedom (DOF)	Mean squares (MS)	*F* (ANOVA)
Rocks	4379.2711	3	1459.7570	29.0511
Rocks>position (Error 1)	1004.9590	20	50.2480	4.5367
Time	33.3146	3	11.1049	1.0026
Interaction: time-rock types	617.8073	9	68.6453	6.1977
Error 2	664.5584	60	11.0760	
Total	6699.9103	95		

Table 4
Microstructural characteristics to be observed in quartz-rich rocks to evaluate their behaviour with respect to the ASR (classification and characteristics based on Passchier and Trouw, 2005; Sibson, 1977, 1990; Spry, 1969 and Vernon, 2004). Depth: approximate depth in crust (km).

Main fault rocks		Deformation regime	Depth (km)	Relevant microstructural characteristics	Potential alkali reactivity of the rock
Breccias and fault gouges (without cohesion)		Brittle deformation	1–4	Crushing along grain boundaries as the grains slide and crack by friction. Plastic deformation is very scarce, some cataclasites present undulatory extinction, lamellar deformation and very incipient grain boundary recrystallisation.	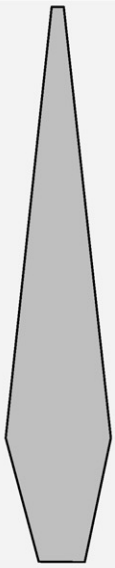
Cataclasites (with cohesion)		Brittle to brittle-ductile deformation	10–15		
Mylonites (with cohesion and foliation)	Protomylonite	Dominant ductile deformation	>10	As deformation intensity progresses, the presence of deformation lamellae, deformation bands and number of subgrains increase. At higher temperature small and new grains grow at the expense of old ones. Marked foliation as the deformation process advances	
	Mylonite (orthomylonite)				
	Ultramylonite				
Pseudotachylytes (with cohesion)		Brittle to brittle-ductile deformation	4–15	Glassy rock with small fragments of the original material.	
Recrystallised rocks	Mynolitic gneiss (low recrystallisation)	Recrystallisation prevails over ductile deformation	>15	Recrystallisation prevails. Formation of new and small grains with subsequent dislocation removal. Marked foliation.	
	Blastomylonite (high recrystallisation)	Recrystallisation prevails over ductile deformation			

References

Andersen, K.T., Thaulow, N., 1989. The application of undulatory extinction angles (UEA) as an indicator of alkali-silica reactivity of concrete aggregates. In: Okada, K., Nishibayashi, S., Kawamura, M. (Eds.), 8th International Conference on Alkali-Aggregate Reaction in Concrete, Kyoto, pp. 489–494.

ASTM C 289, 1994. Potential Alkali–Silica Reactivity of Aggregates (Chemical Method). Annual Book of ASTM Standards. ASTM Publication Office, Philadelphia, PA.

ASTM C 1260, 2005. Standard Test Method for Potential Alkali Reactivity of Aggregates (Mortar-Bar Method). Annual Book of ASTM Standards. American Society for Testing and Materials, West Conshohocken, Pennsylvania.

Baldo, E.G., Casquet, C., Galindo, C., 1996. El metamorfismo de la Sierra Chica de Córdoba (Sierras Pampeanas). Argentina. Geogaceta 19, 51–54.

Batic, O., Sota, J., Cortelezzi, C., Pavlicevic, R., 1987. Experiencias sobre la reactividad deletérea de algunas rocas graníticas. 8va Reunión Técnica de la AATH, pp. 19-27.

Batic, O.R., Sota, J.D., Falcone, D.D., 2008. Caracterización de los agregados de nuestro país frente a la RAS. Memorias del 1º Congreso Argentino de Áridos, Mar del Plata, Buenos Aires, Tomo I, pp. 419-426.

Best, M.G., 2003. Igneous and Metamorphic Petrology, second ed. Blackwell Science Ltd., Oxford.

Bonalumi, A.A., Escayola, M., Kraemer, P.E., Baldo, E.G., Martino, R.D., 1999. Precámbrico-Paleozoico inferior de las Sierras de Córdoba. In: Caminos, R. (Ed.), Geología Argentina. Anales 29, Instituto de Geología y Recursos Minerales, SEGEMAR, Buenos Aires, Capítulo 6, pp. 136–140.

Broekmans, M.A.T.M., 2004a. Qualities of quartz and the alkali-silica reaction in concrete. In: Pecchio, M., et al. (Ed.), Proceedings 8th International Congress on Applied Mineralogy, Brazil, pp. 661–664.

Broekmans, M.A.T.M., 2004b. Structural properties of quartz and their potential role for ASR. Mater. Charact. 53, 129–140.

Broekmans, M.A.T.M., 2004c. The Crystallinity Index of Quartz by XRD, Its Susceptibility for ASR, and a Brief Methodological Review. In: Tang, Deng, M. (Eds.), 12th International Conference on Alkali-Aggregate Reaction in Concrete. Academic Publisher, Beijing, China, pp. 60–68.

Brown, L.S., 1955. Some observations on the mechanics of alkali-aggregate reaction. ASTM Bull. 205, 40.

Chalmers, B., 1959. Physical Metallurgy. Wiley, New York.

CIRSOC 201, 2005. Reglamento Argentino de Estructuras de Hormigón (Proyecto en trámite de aprobación). Centro de Investigación de los Reglamentos Nacionales de Seguridad para las Obras Civiles (CIRSOC), Sistema INTI. http://www.inti.gov.ar/cirsoc/.

Cortelezzi, C.R., Maiza, P., Pavlicevic, R.E., 1990. Strained quartz in relation to alkali-silica reaction. In: Erlin, B., Stark, D. (Eds.), Petrography Applied to Concrete and Concrete Aggregates. ASTM STP 1061, Philadelphia, pp. 145–158.

Dehills, M.S., Corvalan, J., 1964. Undulatory extinction in quartz grains of some Chilean granitic rocks of different ages. Geol. Soc. Am. Bull. 75, 363–366.

Dolar-Mantuani, L.M.M., 1981. Undulatory extinction in quartz used for identifying potentially alkali-reactive rocks. In: Oberholster, R.E. (Ed.), 5th International Conference on Alkali-Aggregate Reaction in Concrete, S252/36, Cape Town, South Africa, pp. 1–6.

Falcone, D.D., Sota, J.D., Batic, O.R., 2008. Discusión sobre métodos para evaluar agregados potencialmente reactivos. Memorias del III Congreso Internacional de la AATH, 17ª Reunión Técnica, Córdoba, pp. 329–336.

French, W.J., 1991. Concrete petrography: a review. Q. J. Eng. Geol. 24, 17–48.

French, W.J., 1992. The characterization of potentially reactive aggregates. In: Poole, A.B. (Ed.), 9th International Conference on Alkali-Aggregate Reaction in Concrete, Conc. Soc. Publ. CS.104 1, London, pp. 338–346.

García del Amo, D., Calvo Pérez, B., 2001. Diagnosis of the alkali-silica reactivity potential by means of digital image analysis of aggregate thin sections. Cem. Concr. Res. 31, 1449–1454.

Giaccio, G., Zerbino, R., Ponce, J.M., Batic, O.R., 2008. Mechanical behavior of concretes damaged by alkali-silica reaction. Cem. Concr. Res. 38, 993–1004.

Gogte, B.C., 1973. An evaluation of some common Indian rocks with special reference to alkali-aggregate reactions. Eng. Geol. 7, 135–153.

Gordillo, E.C., 1958. Estudio químico-petrográfico de las rocas intrusivas de la Quebrada del Río Primero, Córdoba, Argentina. Boletín de la Academia Nacional de Ciencias, Tomo, vol. 40, pp. 141–170.

Gordillo, C.E., Lencinas, A.N., 1979. Sierras Pampeanas de Córdoba y San Luis. In: Turner, J.C.M. (Ed.), Segundo Simposio Geología Regional Argentina, Academia Nacional de Ciencias, Tomo I, Córdoba, pp. 577–650.

Grattan-Bellew, P.E., 1986. Is high undulatory extinction in quartz indicative of alkali-expansivity of granitic aggregates? In: Grattan-Bellew, P.E. (Ed.), 7th International Conference on Alkali-Aggregate Reaction in Concrete, Ottawa, Canada. Noyes Publications, Park Ridge, N. J, pp. 434–439.

Grattan-Bellew, P.E., 1992. Microcrystalline quartz, undulatory extinction and the alkali-silica reaction. In: Poole, A.B. (Ed.), 9th International Conference on Alkali-Aggregate Reaction in Concrete, Conc. Soc. Publ. CS.104 1, London, pp. 383–394. 1992.

Hirt, G., Tullis, J., 1992. Dislocation creep regimes in quartz aggregates. J. Struct. Geol. 14 (2), 145–159.

Hobbs, B.E., Means, W.D., Williams, P.F., 1976. An Outline of Structural Geology. John Wiley and Sons, New York.

Hull, D., 1975. Introduction to Dislocations. Pergamon Press, Oxford.

Hünger, K.-J., 2007. The contribution of quartz and the role of aluminum for understanding the AAR with greywacke. Cem. Concr. Res. 37, 1193–1205.

Ichikawa, T., Miura, M., 2007. Modified model of alkali-silica reaction. Cem. Concr. Res. 37, 1291–1297.

Katayama, T., Futagawa, T., 1989. Alkali-Aggregate Reaction in New Brunswick, Eastern Canada—Petrographic Diagnosis of the Deterioration. In: Okada, K., Nishibayashi, S., Kawamura, M. (Eds.), 8th International Conference on Alkali-Aggregate Reaction in Concrete, Kyoto, pp. 531–536.

Kerrick, D.M., Hooton, R.D., 1992. ASR of concrete aggregate quarried from a fault zone: results and petrographic interpretation of accelerated mortar bar test. Cem. Concr. Res. 22, 949–960.

Kingery, W.D., 1960. Introduction to Ceramics. Wiley, New York.

Lagerblad, B., Trägårdh, J., 1992. Alkalisilikareaktioner i svensk betong (Alkali-silica reactions in Swedish concrete). CBI Rapport 4:92. Cement och Betong Institutet, Stockholm, p. 74.

Locati, F., Marfil, S., Baldo, E., Batic, O., 2008. Comportamiento de rocas metamórficas con venas de pseudotaquilitas de las Sierras Chicas de Córdoba, frente a la reacción

álcali-sílice. Memorias del III Congreso Internacional de la Asociación Argentina de Tecnología del Hormigón, 17ª Reunión Técnica, Córdoba, pp. 257–264.
Maiza, P.J., Salomón, R.C., Marfil, S.A., 1999. Susceptibilidad a la corrosión de agregados pétreos para hormigón a partir del estudio sobre superficies pulidas. XIV Congreso Geológico Argentino, Salta, Actas II, pp. 416–418.
Marfil, S.A., Maiza, P.J., 2001. Deteriorated pavements due to the alkali-silica reaction. A petrographic study of three cases in Argentina. Cem. Concr. Res. 31, 1017–1021.
Marfil, S.A., Maiza, P.J., Salomón, R.C.J., 1998. Evaluación de la corrosión superficial de un agregado cuarcítico en un medio alcalino mediante el estudio estadístico de imágenes digitalizadas. Revista Hormigón 32, 11–16.
Menegon, L., Pennacchioni, G., Heilbronner, R., Pittarello, L., 2008. Evolution of quartz microstructure and c-axis crystallographic preferred orientation within ductilely deformed granitoids (Arolla unit, Western Alps). J. Struct. Geol. 30, 1332–1347.
Mielenz, R.C., 1954. Petrographic examination of concrete aggregate. ASTM Proc. 54, 1188–1218.
Mielenz, R.C., 1958. Petrographic Examination of Concrete Aggregate to Determine Potential Alkali-Reactivity. Report No. 18-C, Highway (Transportation) Res. Board, 29-38.
Morino, K., 1986. Alkali aggregate reactivity of cherty rock. Concrete alkali-aggregate reaction. In: Grattan-Bellew, P.E. (Ed.), 7th International Conference on Alkali-Aggregate Reaction in Concrete, Ottawa, Canada. Noyes Publications, Park Ridge, NJ, pp. 501–506.
Murata, K.J., Norman, M.B., 1976. An index of crystallinity for quartz. Am. J. Sci. 276, 1120–1130.
Passchier, C.W., Trouw, R.A.J., 2005. Microtectonics, second ed. Springer-Verlag, Berlin.
Poirier, J.-P., 1985. Creep of Crystals. High Temperature Deformation Processes in Metals, Ceramics and Minerals. Cambridge University Press, Cambridge, MA.
Poirier, J.-P., Guillopé, M., 1979. Deformation induced recrystallisation of minerals. Bull. Minéral. 102, 67–74.
Ponce, J.M., Batic, O.R., 2006. Different manifestations of the alkali-silica reaction in concrete according to the reaction kinetics of the reactive aggregate. Cem. Concr. Res. 36, 1148–1156.
Rapela, C.W., Pankhurst, R.J., Casquet, C., Baldo, E., Saavedra, J., Galindo, C., Fanning, C.M., 1998. The Pampean Orogeny of the southern proto-Andes: Cambrian continental collision in the Sierras de Córdoba. In: Pankhurst, R.J., Rapela, C.W. (Eds.), The Proto-Andean Margin of Gondwana: Geol. Soc. London Spec. Publ., vol. 142, pp. 181–217.
Shand, S.J., 1916. the pseudotachylyte of Parijs (Orange Free State), and its relation to 'trap-shotten gneiss' and 'flinty crush-rock'. Q. J. Geol. Soc. 72 (1–4), 198–221.
Sibson, R.H., 1977. Fault rocks and fault mechanisms. J. Geol. Soc. London 133, 191–214.
Sibson, R.H., 1990. Faulting and fluid flow. In: Nesbitt, B.E. (Ed.), Fluids in tectonically active regimes of the continental crust: Mineralogical Association of Canada Short Course, vol. 18, pp. 93–132.
Spry, A., 1969. Metamorphic Textures. Pergamon Press, Oxford.
St. John, D.A., Poole, A.W., Sims, I., 1998. Concrete Petrography. A Handbook of Investigative Techniques. Arnold, Great Britain.
Stanton, T.E., 1940a. Expansion of concrete through reaction between cement and aggregate. Proc. Am. Soc. Civ. Eng. 66, 1781–1811.
Stanton, T.E., 1940b. Influence of cement and aggregate on concrete expansion. Eng. News-Record 124 (5), 59–61.
Steel, R.G.D., Torrie, J.H., 1981. Principles and procedures of statistics. Mc. Graw Hill, Singapore.
Thomson, M.L., Grattan-Bellew, P.E., 1993. Anatomy of a porphyroblastic schist: alkali-silica reactivity. Eng. Geol. 35, 81–91.
Thomson, M.L., Grattan-Bellew, P.E., White, J.C., 1994. Application of microscopic and XRD techniques to investigate alkali-silica reactivity potential of rocks and minerals. In: Gouda, G.R., Nisperos, A., Bayles, J. (Eds.), Proceedings of the 16th International Conference on Cement Microscopy. International Cement Microscopy Association, Texas, pp. 174–192.
Urai, J.L., Means, W.D., Lister, G.S., 1986. Dynamic recrystallization of minerals. In: Hobbs, B.E., Heard, H.C. (Eds.), Mineral and Rock Deformation: Laboratory Studies: American Geophysical Union, Geophysical Monograph 36, Washington D.C., pp. 161–200.
Vernon, R.H., 2004. A Practical Guide to Rock Microstructure. Cambridge Univ Press, United Kingdom.
Wakizaka, Y., 2000. Alkali-silica reactivity of Japanese rocks. Eng. Geol. 56, 211–221.
Wang, Z., Cheng, Q., Cao, L., Xia, Q., Chen, Z., 2007. Fractal modelling of the microstructure property of quartz mylonite during deformation process. Math. Geol. 39 (1), 53–68.
Wenk, H.-R., Monteiro, P.J.M., Shomglin, K., 2008. Relationship between aggregate microstructure and mortar expansion. A case study of deformed granitic rocks from the Santa Rosa mylonite zone. J. Mater. Sci. 43, 1278–1285.
West, G., 1991. A note on undulatory extinction of quartz in granite. Q. J. Eng. Geol. Hydrogeol. 24, 159–165.
West, G., 1994. Undulatory extinction of quartz in some British granites in relation to age and potential reactivity. Q. J. Eng. Geol. Hydrogeol. 27, 69–74.
White, S., 1973. The dislocation structures responsible for the optical effects in some naturally-deformed quartzes. J. Mater. Sci. 8, 490–499.
Wigum, B.J., 1995. Examination of microstructural features of Norwegian cataclastic rocks and their use for predicting alkali-reactivity in concrete. Eng. Geol. 40, 195–214.
Wigum, B.J., French, W.J., 1996. Sequential examination of slowly expanding alkali-reactive aggregates in accelerated mortar bar testing. Mag. Concr. Res. 48 (177), 281–292.
Wigum, B.J., Lindgård, J., 1994. Test methods for alkali aggregate reactions in Norwegian aggregates: petrographic examination and the South African NBRI Mortar-Bar Test. In: Malhotra, V.M. (Ed.), Durability of Concrete, 3rd International Conference on Alkali-Aggregate Reaction in Concrete, ACI SP-145. Nice, France, pp. 781–796.
Wigum, B.J., Pedersen, L.T., Grelk, B., Lindgård, J., 2006. State-of-the art report: key parameters influencing the alkali aggregate reaction. SINTEF report, SBF52 A06018, p. 131.
Zhang, X., Blackwell, B.Q., Groves, G.W., 1990. The microstructures of reactive aggregates. Br. Ceram. Trans. J. 89, 89–92.